Spectrum of Engineering Sciences
ISSN (e) 3007-3138 (p) 3007-312X Volume 3, Issue 11, 2025

STRUCTURAL, OPTICAL AND ELECTRICAL PROPERTIES OF CUINGASE2 (CIGS) THIN FILMS TO BE USED AS ABSORBER LAYER IN SOLAR CELLS

Humaira Ramzan[1], Huda Shahid[2], Nazeer Abbas khan[3], Iqra Ashraf[4], Nizam Ahmad[5] Shanza Taswar[6], Faisal Amin[*7]

[1,2,4,5,*7] *Centre of excellence in solid state physics University of the Punjab, Lahore, Pakistan.*
[3]*Centre for micro mechanics modelling andcharacterisation Harbin Institute of technology Shenzhen*
[6]*School of Materials Science and Engineering, Harbin Institute of Technology (Shenzhen), Shenzhen*

[1]humairaramzan86@gmail.com, [2]huda.cssp@gmail.com, [3]25bf58043@stu.hit.edu.com
[4]Iqraashraf.bzu@gmail.com, [5]nizamah17@gmail.com, [6]shanzayirfan99@gmail.com,
[*7]engr.mfa.fs@gmail.com

DOI:https://doi.org/10.5281/zenodo.17679709

Keywords
CIGS Thin Films, Electrodeposition, Absorber Layer, Structural Properties, Optical Properties, X-ray Diffraction (XRD), Spectroscopic Ellipsometry, Band Gap Engineering, Hall Effect Measurements, Thin-Film Solar Cells.

Article History
Received: 01 October 2025
Accepted: 10 November 2025
Published: 22 November 2025

Corresponding Author: *
Faisal Amin

Abstract
Electrodeposition method is used in the present study to prepare thin films of copper indium gallium di selenide ($CuInGaSe_2$) using ITO coated glass substrates. Properties of $CuInGaSe_2$ thin films have been optimized for their potential use as an absorber layer in solar cell. Cyclic Voltameter is used to determine the reduction potentials of metals. The reduction potential value is observed in the range of 0.5 to 0.9 V. Electrodeposition process is used to prepare the five sample by varying the reduction potential applied during the process of electrodeposition. X-ray Diffraction (XRD), spectroscopic ellipsometer and Hall measurements are used to study the structural optical and electrical properties of the sample deposited on substrate as a thin film. $CuInGaSe_2$ thin films, prepared and deposited at 0.5V and 0.6 V, exhibit mixed crystal phases. Whereas, single phase $CuInGaSe_2$ structure is observed with the increase in voltage to 0.7 V. XRD confirm the tetragonal structure of $CuInGaSe_2$ thin film prepared by electrodeposition process. Single phase structure persist with the further increase in voltage to 0.8V to 0.9V, however, reduced crystallite size along with increased dislocation density is observed at higher deposition voltages. Optical properties show that the electrodeposited thin films are capable to absorb maximum part of solar spectrum. The fundamental absorption edge is appeared at 1070 nm. Value of the direct band gap observed is ~1.16eV. Temperature dependent Hall measurements are performed for the thin films prepared with 0.7 V. High value of conductivity, low resistivity, high mobility and large value of carrier concentration are observed at ~315K.

INTRODUCTION

The global energy landscape is undergoing a significant transformation, driven by the increasing demand for power and the pressing need to mitigate the environmental impact of conventional fossil

fuels. In this context, scientific inquiry has intensified around renewable energy resources, which offer a sustainable and clean alternative [1]. Solar energy, being the most abundant renewable source, holds the paramount potential to meet a substantial portion of the world's energy requirements. The direct conversion of sunlight into electrical energy via photovoltaic (PV) technology is a cornerstone of this solar energy harnessing [2].

The efficacy of a photovoltaic device is intrinsically linked to its ability to absorb incident solar radiation. The solar spectrum approximates a black body radiator at 6050 K, with approximately 98% of its energy distributed within the wavelength range of 0.25 to 3.0 μm [3]. The industry standard for evaluating solar cell performance is the Air Mass 1.5 Global (AM 1.5G) spectrum, representative of sunlight after traversing 1.5 atmospheres and possessing a power density of 100 mW/cm² [4]. An ideal photovoltaic absorber material must exhibit a high absorption coefficient across this spectral range to maximize photon capture and conversion.

While crystalline silicon has been the workhorse of the PV industry, its inherent material properties impose limitations, including an indirect bandgap (~1.1 eV) that necessitates the use of thick, mechanically robust wafers to achieve sufficient light absorption, thereby increasing material costs and limiting application flexibility [5]. These constraints have catalyzed the development of thin-film photovoltaic technologies, which promise reduced material usage, lower manufacturing costs, and new application possibilities. Among the prominent thin-film candidates, Cadmium Telluride (CdTe) and Gallium Arsenide (GaAs) have been widely studied. However, GaAs is associated with high production costs [6] while CdTe involves the use of toxic cadmium, raising environmental concerns [7].

Copper Indium Gallium Selenide ($Cu(In,Ga)Se_2$ or CIGS) has emerged as a leading material for high-performance thin-film photovoltaics. This I-III-VI_2 group quaternary compound semiconductor possesses a direct, tunable bandgap, which can be optimally aligned with the solar spectrum by varying the gallium-to-indium (Ga/(In+Ga)) ratio, typically yielding values between 1.01 eV and 1.68 eV [8]. Furthermore, CIGS exhibits an exceptionally high absorption coefficient (>10^5 cm^{-1}), allowing for near-complete light absorption within an absorber layer thickness of just 1-2 micrometers [9]. These properties, coupled with demonstrated laboratory-scale power conversion efficiencies exceeding 22.6%, establish CIGS as a highly promising absorber material for cost-effective and high-efficiency solar cells [10].

A typical CIGS solar cell is fabricated in a substrate configuration, as illustrated in **Fig. 1.1**. The standard device stack comprises a soda-lime glass substrate, a sputtered Molybdenum (Mo) back-contact layer, the p-type CIGS absorber layer, an n-type buffer layer (often CdS deposited via chemical bath deposition), and a front transparent conducting oxide window layer such as intrinsic and Al-doped ZnO (i-ZnO/ZnO:Al) [11]. A critical challenge for the widespread commercialization of CIGS technology remains the development of deposition techniques that are both scalable to large areas and capable of producing high-quality, electronically superior absorber layers at a low cost.

This research work focuses on the synthesis of CIGS thin films using the electrodeposition method a non-vacuum, cost-effective, and readily scalable technique. The primary objective is to systematically optimize the key properties of electrodeposited CIGS films on ITO-coated glass substrates by varying the critical parameter of applied deposition potential. The structural, optical, and electrical properties of the resulting films are thoroughly characterized to evaluate their suitability for integration as an efficient absorber layer in thin-film solar cells.

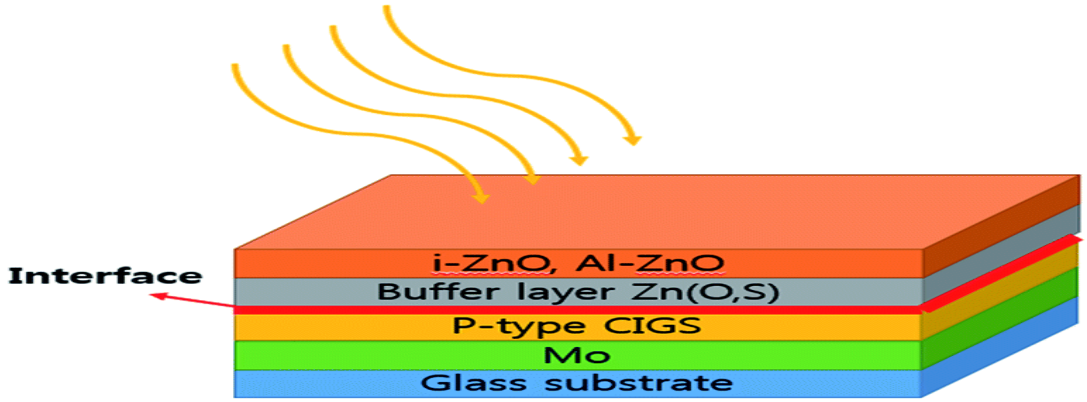

Fig 1.11: CIGS Solar cell layer Structure

2.Existing Literature

The optimization of Copper Indium Gallium Selenide (CIGS) thin films for solar cell applications is a widely researched area, with significant focus on deposition techniques, substrate engineering, and post-treatment processes to enhance device performance. Recent studies highlight various innovative approaches.

[12] demonstrated an efficiency improvement in electrodeposited CIGS solar cells by spin-coating a wide-bandgap In_2S_3 thin film as a buffer layer. The In_2S_3 layer, derived from a precursor solution of $InCl_3$ and thiourea in dimethyl sulfoxide, replaced the traditional CdS layer, leading to a superior device structure. The resulting cell, with a Mo/CIGS/In_2S_3/i-ZnO/Al-ZnO/Ni-Al configuration, showed enhanced performance, characterized using X-ray photoelectron spectroscopy (XPS).Substrate choice and alkali doping are critical for CIGS performance.[13] investigated bifacial semi-transparent ultra-thin CIGS solar cells fabricated on ITO substrates. Their work emphasized the influence of ITO thickness and Na doping, using alkali-free glass for controlled Na incorporation. They concluded that effective light management strategies are vital for such devices, opening avenues for applications in solar windows and building-integrated photovoltaics. Similarly, [14] developed ultrathin CIGS solar cells on ITO-coated glass using a single-stage co-evaporation process, achieving uniform films crucial for transparent photovoltaic applications.The pursuit of cost-effective fabrication methods is a major driver in the field. [15] explored a solution-processing route for CIGS absorbers, emphasizing its advantages in stoichiometric control and high material utilization. They reported that controlling the selenization temperature and elemental composition in precursors allowed for the formation of an Ordered Vacancy Compound (OVC) phase at the surface. This OVC phase, with a lower valence band position, improved carrier collection and reduced interface defect density, leading to significantly higher device efficiency.Advanced deposition strategies combining multiple techniques have also been explored. [16] employed a hybrid method involving both vacuum and non-vacuum processes to fabricate CIGS absorbers. This approach minimized material waste while achieving a high efficiency of 21.92%. Their study provided a detailed analysis of the optimized parameters and defect control necessary for high-performance CdS/CIGS heterojunctions.Post-deposition treatments (PDT) with alkali metals have proven highly effective. [17] evaluated the impact of CsF-PDT on CIGS absorbers. Their comparative study between CdS-covered and bare CIGS surfaces subjected to CsF treatment revealed profound changes in the absorber's electronic properties, contributing to enhanced device performance. [18] provided a comprehensive review of alkali incorporation (Na, K, Rb) in CIGS, detailing the chemical and electrical roles these elements play in boosting efficiency towards theoretical limits.

Beyond photovoltaics, the application of CIGS has been extended to other fields. [19] utilized a CIGS-based photocathode for the photoelectrochemical (PEC) reduction of CO_2 to CO. The standard device structure (Mo/CIGS/CdS/i-ZnO/ZnO:Al) demonstrated the material's potential in solar fuel generation, with performance determined by its light absorption, charge separation, and charge transfer efficiencies.Finally, interface passivation has emerged as a key strategy for performance gains. [20] investigated the use of an Al_2O_3 layer as a front passivation layer on CIGS. They found that inserting an Al_2O_3 tunneling layer between the CIGS absorber and the CdS buffer layer resulted in a very low concentration of interface defects while maintaining bulk recombination channels. This suggests Al_2O_3 is a promising candidate for use with alternative, non-toxic buffer layers.In summary, the current literature underscores a multi-faceted approach to advancing CIGS technology focusing on novel deposition methods, substrate engineering, alkali doping, and interface passivation. This study contributes to this field by exploring the potential of the cost-effective electrodeposition technique to fabricate high-quality CIGS absorber layers.

3. Experimental and Characterization Techniques

3.1 Synthesis of Thin Films

Two primary methodologies exist for thin-film fabrication: physical and chemical processes. Physical processes, such as Physical Vapor Deposition (PVD) require a vacuum environment for deposition. Chemical processes, including Chemical Vapor Deposition (CVD) and plating techniques like electrodeposition, rely on chemical reactions at the substrate surface. For this study, the electrodeposition method was selected due to its cost-effectiveness, simplicity, and the fact that it is a non-vacuum technique that does not require post-deposition annealing.

3.2 Electrodeposition Setup and Methodology

The chemical electrodeposition process utilized several key instruments: an electronic balance (**Fig. 3.1**), a hot plate (**Fig. 3.2**), a magnetic stirrer (**Fig. 3.3**), beakers (**Fig. 3.4**), and a fume hood (**Fig. 3.5**).these figures are shown below. The core of the setup was a three-electrode electroplating cell, consisting of a graphite anode, an ITO-coated glass substrate as the cathode, and a Coleman reference electrode.

Fig 3.1: Electronic Balance

Fig 3.2: Hot Plate

Fig 3.3: Magnetic Stirrer

Fig 3.4 : Beakers of Different Sizes

The principle of electrodeposition is based on the electrolysis of an electrolyte solution. When an external electric field is applied, cations migrate to the cathode and anions to the anode, leading to the deposition of the desired material onto the substrate.

Several factors critically affect the electrodeposition quality:

- **Substrate:** Requires a clean and smooth surface.
- **Temperature:** Operates within a range of 20–70°C.
- **Stirring:** A magnetic stirrer ensures a homogeneous solution.
- **pH:** Influences the deposition process.
- **Applied Current:** Directly proportional to the deposited film's thickness

3.3 Substrate Preparation and Deposition

An ITO-coated glass substrate was chosen for its low cost and high conductivity. Prior to deposition, the substrate underwent a rigorous cleaning process to remove contaminants, which is crucial for uniform film adhesion. This involved sequential ultrasonic baths in acetone (**Fig. 3.5**) and isopropyl alcohol (IPA) (**Fig. 3.6**) each for 30 minutes.

Fig 3.5 Ultrasonic Bath of Acetone

Fig 3.6: Ultrasonic Bath of IPA

The electrolyte was prepared as 0.1 M aqueous solutions of chloride salts of Copper, Indium, Gallium, and Selenide. These solutions were mixed in equal volumes and homogenized using a magnetic stirrer on a hot plate. The deposition was carried out at room temperature by immersing the cleaned substrate in the electrolyte and applying a specific potential for a set duration, with the ITO substrate serving as the cathode. A Cyclic Voltameter (**Fig. 3.7**) was used to determine the suitable reduction potential range for the quaternary system. The overall process flow is summarized in **Fig. 3.8**.

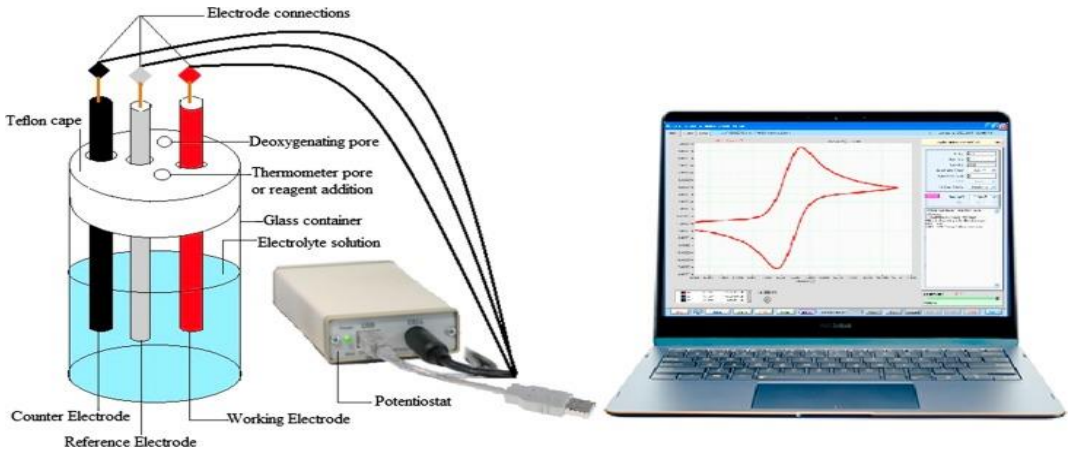

Fig 3.7 Cyclic Voltameter

3.4 Characterization Techniques

The deposited CIGS thin films were characterized using the following techniques to analyze their structural optical and electrical properties:

3.4.1 X-ray Diffraction (XRD)

XRD **(Fig. 3.9)** was used for structural analysis. The technique operates on Bragg's

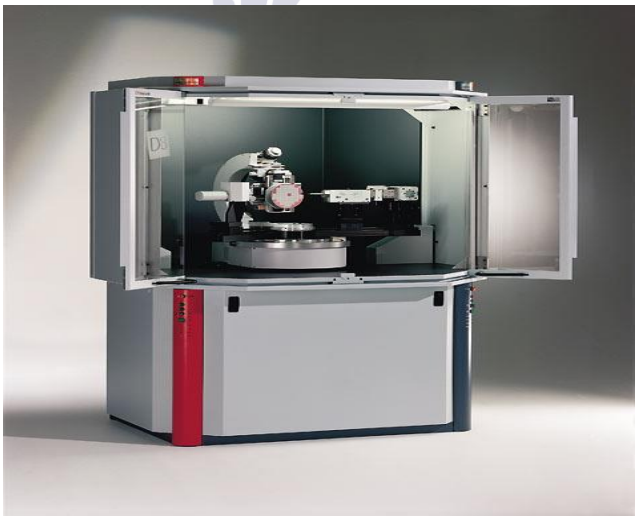

Fig 3.9: XRD Set up (Characterization)

Law:

$$2d \sin\theta = n\lambda \quad \text{.....(3.1)}$$

where d is the interplanar spacing, θ is the Bragg angle, n is the order of reflection,

and λ is the X-ray wavelength. By measuring the diffraction angles and intensities, the crystal structure, phase purity, and other structural parameters of the CIGS films were identified.

3.4.2 Spectroscopic Ellipsometry

This technique (**Figs. 3.10(a) and 3.10(b)**) measures the change in the polarization state of light upon reflection from a sample surface. It was used to determine critical optical properties, including the absorption coefficient and to derive the energy band gap of the thin films.

Fig 3.10(a) Experimental Setup of Spectroscopy Ellipsometer

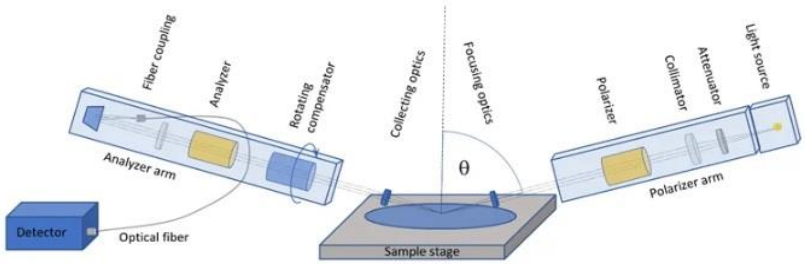

Fig 3.10(b) Parts of Spectroscopy Ellipsometer

3.4.3 Hall Effect Measurements

The Hall effect measurement system was employed to determine the electrical properties of the films. Using the van der Pauw method, this technique provides data on

Carrier concentratio

- Resistivity (ρ)
- Hall mobility (μ)
- Conductivity (σ)

The underlying mechanism is based on the Lorentz force where a magnetic field applied perpendicular to an electric current generates a measurable Hall voltage, from which the electrical parameters are calculated.

4. Results and Discussion

4.1 Structural Analysis

X-ray diffraction (XRD) was employed to analyze the crystal structure of the electrodeposited CIGS thin films. **Figure 4.1** shows the XRD patterns for films

deposited at applied potentials ranging from 0.5V to 0.9V.

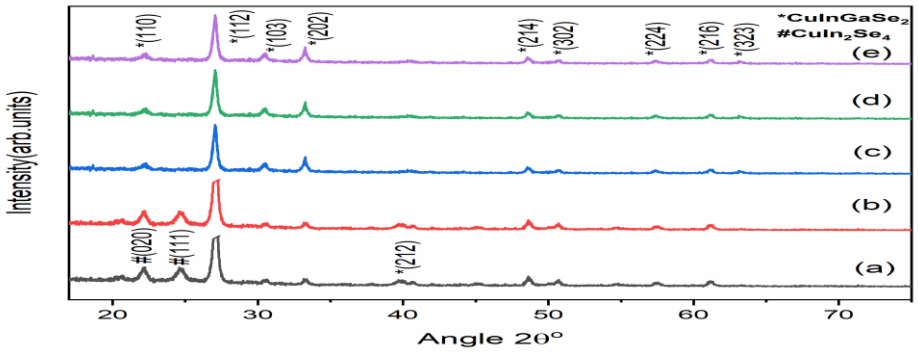

Figure 4.1: XRD patterns of thin films of $CuInGaSe_2$ by varying Potential from (a-e) 0.5 V to 0.9

The results indicate that a single-phase, tetragonal CIGS structure was achieved at 0.7V. Films deposited at lower potentials (0.5V and 0.6V) showed mixed crystal phases, while those at higher potentials (0.8V and 0.9V) maintained the single phase but with reduced crystallinity. The individual XRD patterns for each potential are detailed in **Figures 4.2** through **4.6** with the (112) plane being the most prominent peak confirming the chalcopyrite structure.

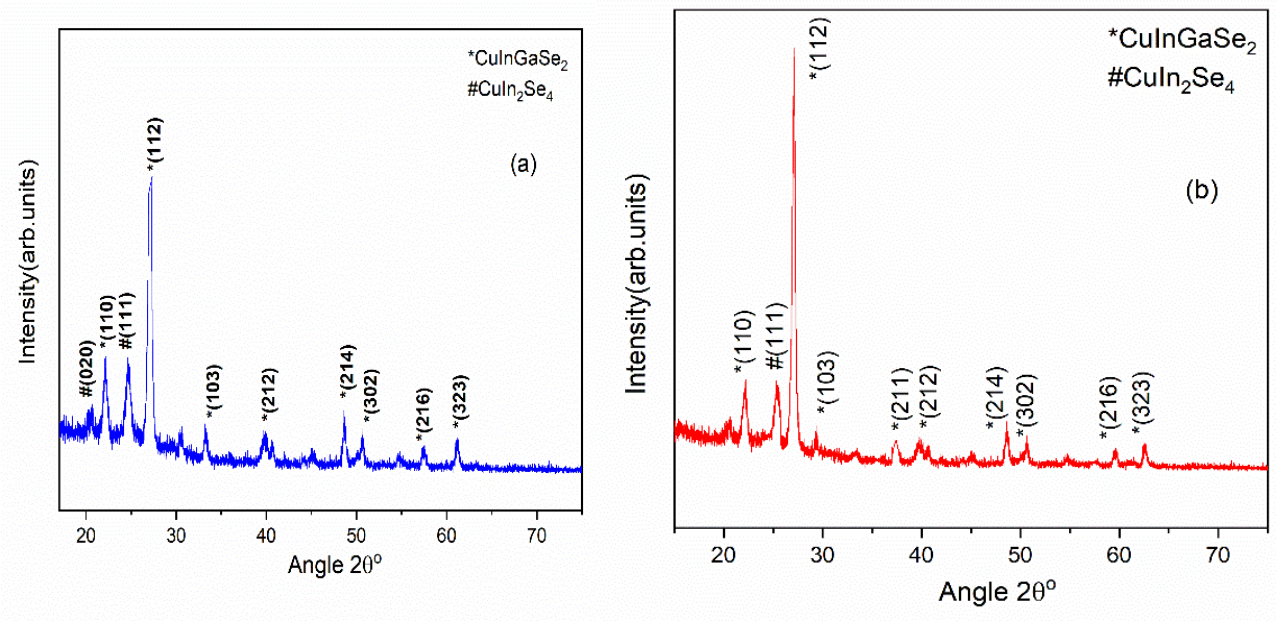

Fig 4.2&3: XRD pattern of thin films prepared with applied potential of 0.5V & 6

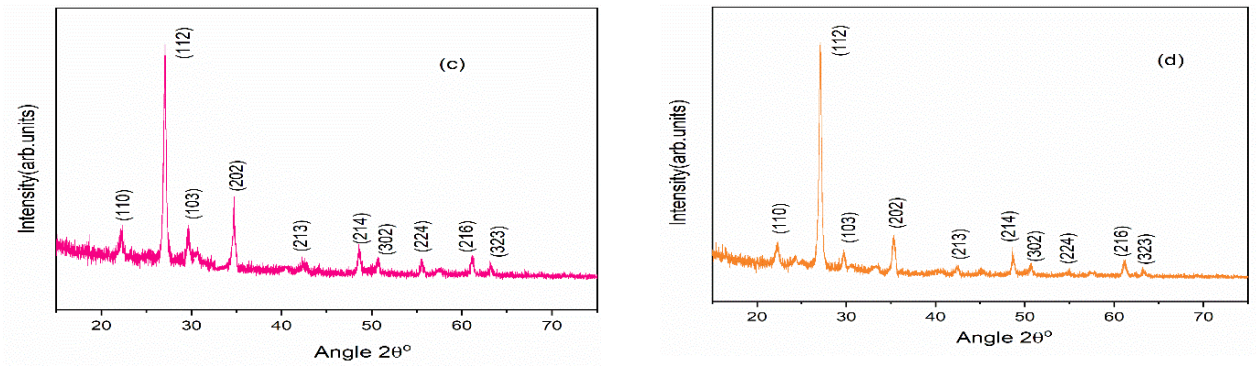

4.4& 5: XRD pattern of thin films prepared with applied potential of 0.8V& 0.7V

The crystallite size (t), dislocation density (δ), and strain (ε) were calculated using the following equations:

$$t = 0.9\lambda / (\beta \cos\theta) \quad \text{.....(4.1)}$$

$$\delta = 1 / t^2 \quad \text{.....(4.2)}$$

$$\varepsilon = \beta / \tan\theta \quad \text{.....(4.3)}$$

where λ is the X-ray wavelength, β is the full width at half maximum, and θ is the Bragg angle.

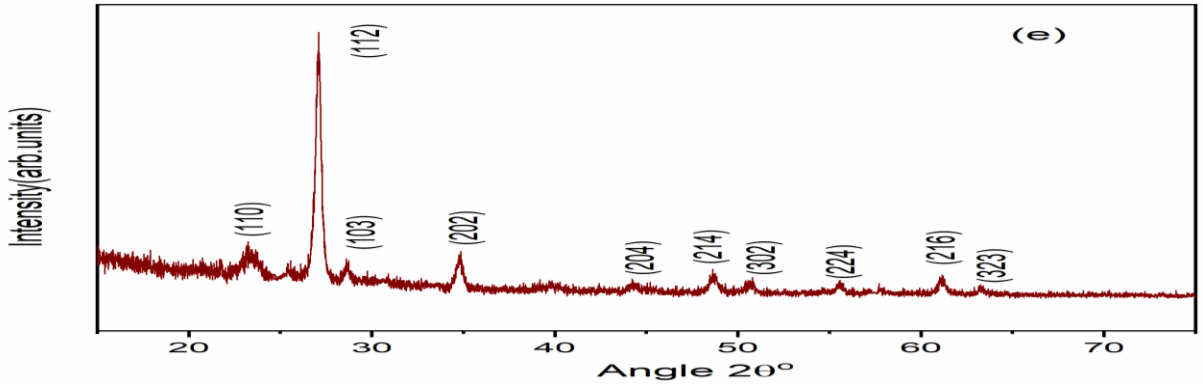

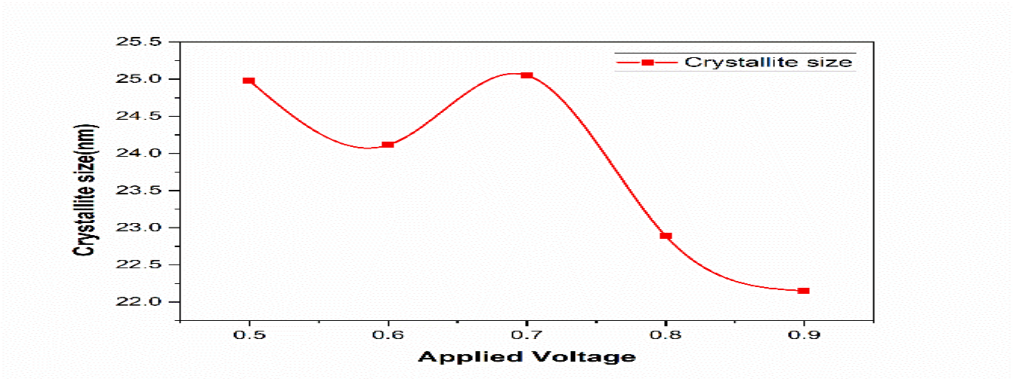

Figure 4.6(b) **illustrates the corresponding dislocation density, which shows an inverse relationship with crystallite size.**

The minimum values of stress/strain and maximum unit cell volume at 0.7V, shown in **Figures 4.6(c)** and **4.6(d)**, indicate the formation of a stable and strengthened crystal structure at this optimized potential.

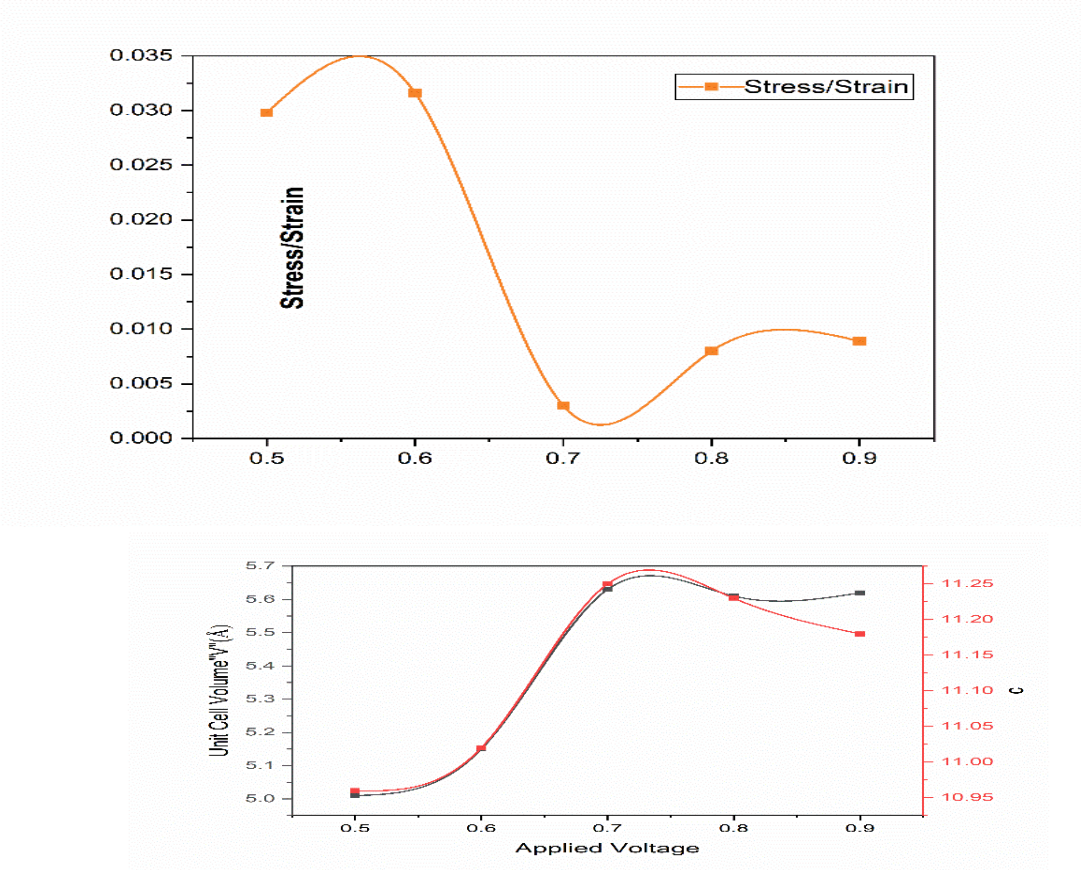

Fig. 4.6(c) Variation in stress/strain and unit cell volume of CIGS thin films Lowest value of stress/strain is observed at 0.7V due to strengthened and stable phase as shown in Fig. 4.6 (d).

4.2 Optical Analysis

4.2.1Transmission and Band Gap Energy

The transmission spectra of the CIGS thin films are presented in Figure 4.7. The absorption edge was observed around 850 nm, shifting with deposition potential.

The sample deposited at 0.7V showed the most favorable absorption characteristics, with high absorption across the visible spectrum and transmission increasing beyond 1100 nm.

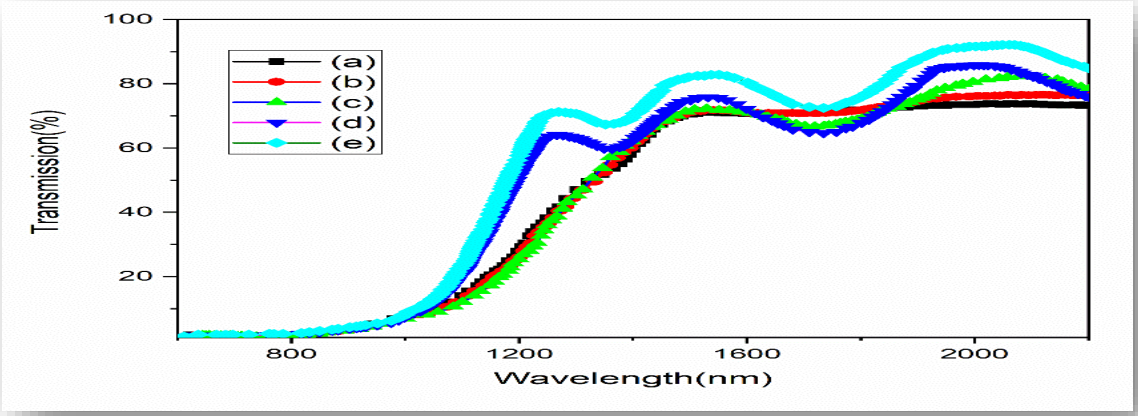

Figure 4.7: Transmittance of CIGS at potential of 0.5V to 0.9V

The absorption coefficient (α) was calculated using the relation:

$$\alpha = (1/t)\ \ln[(2TR^2)/(-(1-R)^2 + \sqrt{(4R^2T^2) + (1-R)^4})] \quad (4.4)$$

where t is thickness, T is transmission, and R is reflection.

The Tauc plots derived from ellipsometry data (**Figure 4.8**) and absorption coefficient analysis (**Figure 4.8 a-e**) confirmed a direct band gap for all samples.The band gap energy variation with deposition potential is summarized in **Figure 4.9**, showing an optimal value of approximately 1.16 eV at 0.7V, which is ideal for solar cell applications.

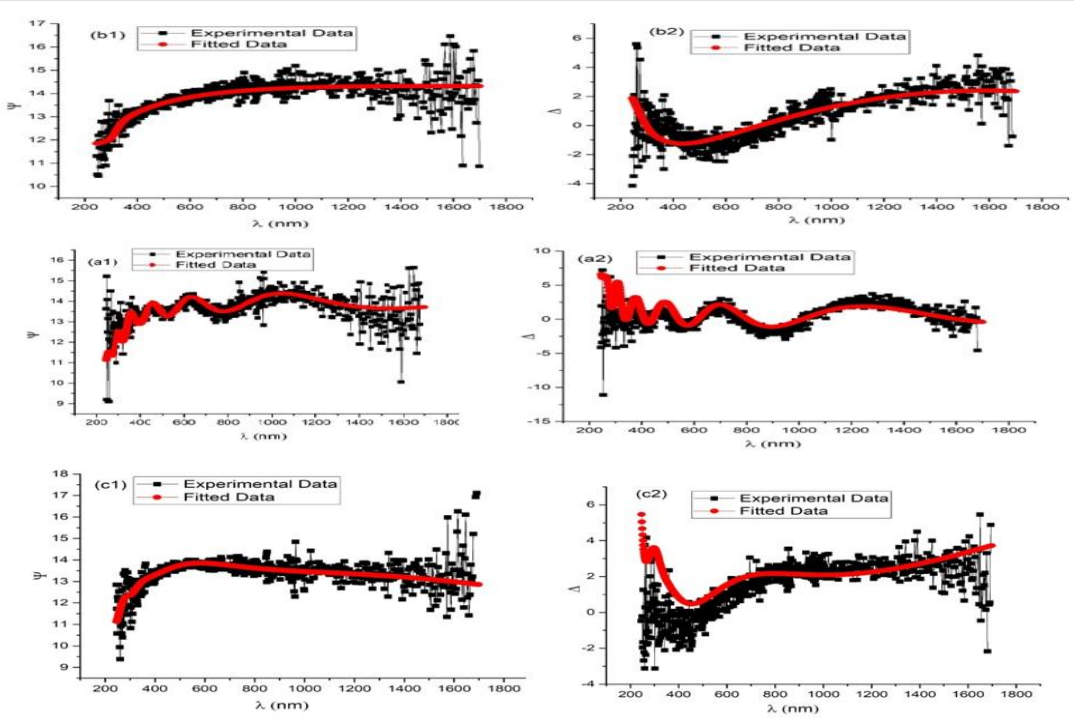

Figure 4.8(a-e): Experimental and fitted ellipsometry plotted with the changes in wavelength

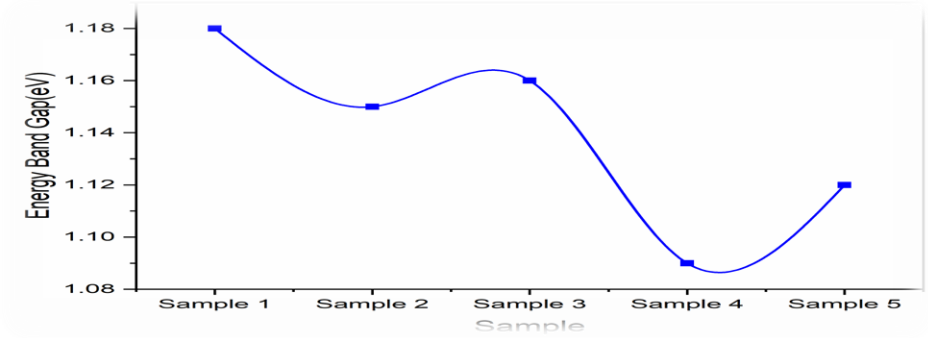

Figure 4.9: Energy band gap variation of CIGS thin films

4.3 Electrical Properties

Temperature-dependent Hall effect measurements were performed on the optimized sample (0.7V). **Figure 4.10** shows the decrease in resistivity with increasing temperature, characteristic of semiconductor behavior.Correspondingly, **Figure 4.11** demonstrates an increase in conductivity with temperature, reaching a maximum of 1.6 $(\Omega \cdot cm)^{-1}$ at 325 K.

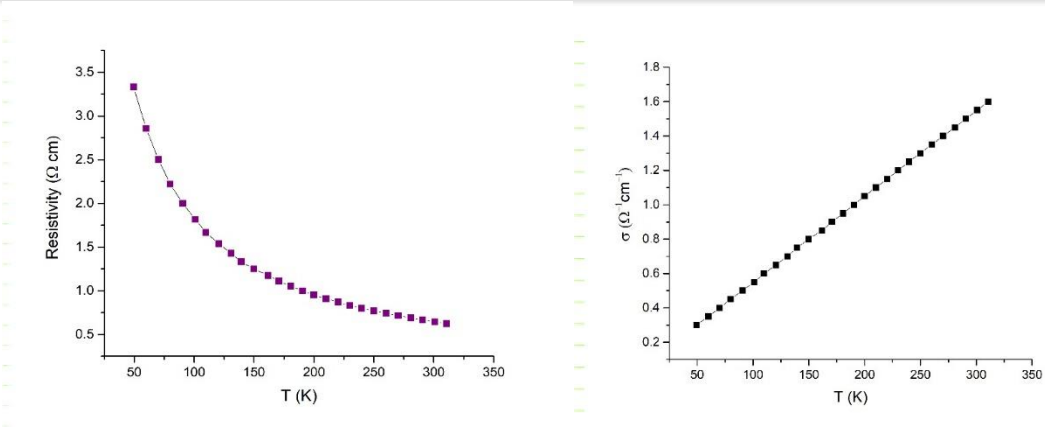

Figure 4.10& 11: Graph betweenconductivity and temperature

The carrier concentration and mobility results are shown in **Figures 4.12** and **4.13**,respectively.

The carrier concentration increases exponentially with temperature due to enhanced thermal generation of electron-hole pairs.

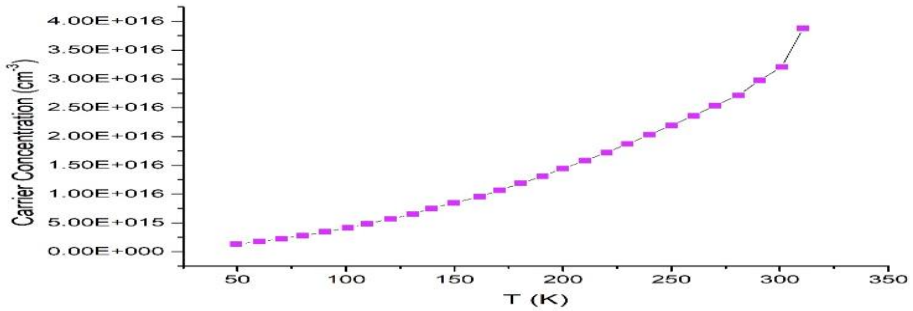

Figure 4.12: Graph between carrier concentration and temperature

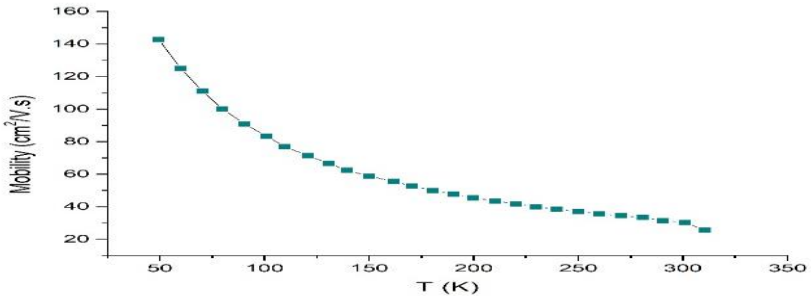

Figure 4.13: Graph between mobility and temperature

Conversely, carrier mobility decreases with rising temperature due to increased scattering

4.4 Overall Performance Optimization

The comprehensive analysis confirms that the CIGS thin film deposited at 0.7V exhibits the most favorable characteristics for solar cell applications:

- Single-phase tetragonal structure with maximum crystallite size
- Optimal direct band gap of ~1.16 eV
- High absorption in the visible spectrum
- Superior electrical properties with high conductivity and carrier concentration

These results validate electrodeposition as a viable, cost-effective method for producing high-quality CIGS absorber layers for photovoltaic devices

5.CONCLUSION

A highly efficient, low cost and application-oriented electrodeposition technique was used for the deposition of thin films of $CuInGaSe_2$ by using ITO coated glass substrate. Applied potential was varied in the range of 0.5 V to 0.9 V. At 0.5 V mixed structure is observed while at 0.7 V the tetragonal structure is observed. The XRD analysis confirmed the tetragonal structure of $CuInGaSe_2$. Spectroscopic Ellipsometry showed that good fit between the experimental and fitted data. The fundamental absorption edge was appeared at 1070 nm. Direct energy bandgap of as low as 1.16 eV was observed. Temperature dependent Hall effect showed the best results of conductivity, resistivity, carrier concentration and mobility for the sample prepared with 0.7V of deposition potential. The results of $CuInGaSe_2$ suggested its use in solar cells. Electrodeposition was the cost effective and non-vacuum technique to prepare CIGS thin film for absorber layer to be used in solar cells.

REFERENCES

A. Curado et al. (2020). Front passivation of $Cu(In,Ga)Se_2$ solar cells using Al_2O_3: Culprits and benefits. *Applied Materials Today*, 21, 100867.

Z. Hu et al. (2020). $Cu(In,Ga)Se_2$ for selective and efficient photoelectrochemical conversion of CO_2 into CO. *Journal of Catalysis*, 384, 88-95.

P. Schoeppe et al. (2020). Revealing the origin of the beneficial effect of cesium in highly efficient $Cu(In,Ga)Se_2$ solar cells. *Nano Energy*, 71, 104622.

Y. Zhao et al. (2021). Controllable formation of ordered vacancy compound for high efficiency solution processed $Cu(In,Ga)Se_2$ solar cells. *Advanced Functional Materials*, 31(10), 2007928.

D. Valencia et al. (2021). Optimization of $Cu(In,Ga)Se_2$ (CIGSe) thin film solar cells parameters through numerical simulation and experimental study. *Solar Energy*, 224, 298-308.

Ochoa et al. (2022). Charge Carrier Lifetime Fluctuations and Performance Evaluation of $Cu(In,Ga)Se_2$ Absorbers via Time-Resolved-Photoluminescence Microscopy. *Advanced Energy Materials*, 12(3), 2102800.

Q. Gao et al. (2022). Efficiency improvement of electrodeposition-processed CIGS solar cell with widen surface bandgap by spin-coating In_2S_3 thin film. *Applied Surface Science*, 578, 152063.

Y. Li et al. (2022). Bifacial semi-transparent ultra-thin $Cu(In,Ga)Se_2$ solar cells on ITO substrate: How ITO thickness and Na doping influence the performance. *Solar Energy Materials and Solar Cells*, 234, 111431.

J. Shin et al. (2022). Ultrathin $Cu(In,Ga)Se_2$ transparent photovoltaics: an alternative to conventional solar energy-harvesting windows. *Nano Energy*, 92, 106711.

Y. Wang et al. (2022). Review on incorporation of alkali elements and their effects in $Cu(In,Ga)Se_2$ solar cells. *Journal of Materials Science & Technology*, 96, 179-189.

S. A. Khalate et al. (2023). A comprehensive review on electrodeposited CIGS thin films: Growth mechanism, challenges, and future perspectives. *Solar Energy*, 262, 111835.

J. Park et al. (2023). Recent progress in non-vacuum electrodeposition of CIGS thin films: A review of developments in electrolyte composition. *Journal of Electroanalytical Chemistry*, 938, 117439.

Zhang et al. (2023). Optimization of electrodeposition potential for high-quality CIGS absorber layers: A comparative structural and optical study. *Thin Solid Films*, 785, 140098.

R. K. Choubey et al. (2023). Impact of deposition voltage on the structural and electrical properties of electrodeposited CIGS thin films for photovoltaic applications. *Materials Science in Semiconductor Processing*, 165, 107654.

H. Liao et al. (2023). Enhancing the efficiency of electrodeposited CIGS solar cells through post-deposition annealing and alkali treatment. *Ceramics International*, 49(15), 25542-25551.

A. Zarkov et al. (2023). Advances in spectroscopic ellipsometry for characterization of thin-film photovoltaic materials. *Applied Surface Science Advances*, 16, 100431.

S. Chen et al. (2024). Bandgap engineering of electrodeposited CIGS thin films by controlled gallium incorporation: A structural and optical perspective. *Solar Energy Materials and Solar Cells*, 268, 112735.

Theelen et al. (2024). Long-term stability of electrodeposited CIGS solar cells: The role of buffer layer and interface engineering. *Progress in Photovoltaics: Research and Applications*, 32(1), 45-58.

Amin et al. (2024). Numerical simulation and experimental validation of electrodeposited CIGS solar cell performance. *Energy Reports*, 10, 2345-2357.

H. C. S. Souza et al. (2024). Green electrodeposition: A review of environmentally friendly electrolytes for CIGS thin film synthesis. *Sustainable Materials and Technologies*, e00845.